Journal of Southeast University (English Edition) Vol. 41, No. 2, pp. 140-146 June 2025 ISSN 1003-7985

# Multiuser transmission scheme in millimeter-wave systems assisted by an RIS subarray

AI Junjie, CHEN Weicong, LIU Jia, CAI Xuefeng, TANG Wankai, JIN Shi

(National Mobile Communications Research Laboratory, Southeast University, Nanjing 211189, China)

**Abstract**: The deployment of reconfigurable intelligent surfaces (RISs) can enhance the coverage ability of millimeter wave (mmWave) communication systems. However, the typical strong line-of-sight (LoS) far-field propagation between a base station (BS) and an RIS reduces channel rank, thus affecting multiuser spatial multiplexing. To address this issue, we propose an RIS subarray-assisted mmWave multiuser transmission scheme. To increase channel rank, RIS is divided into multiple subarrays with adjustable spacing, and the channel is modeled using a hybrid spherical- and planar-wave model. To minimize interuser interference, the RIS subarrays are deployed in the discrete Fourier transform (DFT) direction of the BS antenna array. To maximize signal efficiency, the BS precoder, the RIS reflection coefficients, and the user's combiner are jointly designed. Numerical simulations were conducted to verify the effectiveness of the proposed RIS subarray deployment strategy and the performance of the wireless transmission scheme. In a four-user equipment (UE) communication scenario in the mmWave band, the effective rank of the BS-RIS channel approaches full rank, and the spectral efficiency of each UE is improved by at least 3 bit/(s·Hz).

**Key words**: millimeter waves; reconfigurable intelligent surface (RIS); discrete Fourier transform (DFT) codebook; wireless communications

DOI: 10. 3969/j. issn. 1003-7985. 2025. 02. 002

With the ongoing commercial rollout of the 5th generation (5G) mobile communication system, ensuring secure and stable operation of the industrial Internet in the physical world has become increasingly important[1]. In response, the global industry has embarked on research and investigation of the 6th generation (6G) mobile communication system. The expectations for 6G systems are high; the objective is to enable revolutionary applications, including multisensory extended reality (XR), interconnected robotics and autonomous systems, blockchain and distributed ledger technologies, and wireless brain-computer interaction[2]. The millimeter wave (mmWave) technology is a key technology for 6G systems. By exploiting the abundant frequency resources provided by the mmWave band, the communication bandwidth is substantially expanded, leading to a significant improvement in the peak data rate of communication systems[3-4]. However, due to the propagation characteristics of mmWave communication systems, such as high path loss, weak penetration, and scattering, it is extremely challenging to achieve wide coverage and high-reliability transmission simultaneously. Moreover, the expensive system hardware and high energy consumption impede mmWave practical applications. To achieve the ambitious goals of 6G communication systems at a low cost and low power consumption, it is crucial to introduce transformative technologies.

A reconfigurable intelligent surface (RIS) is an electromagnetic (EM) surface structure consisting of many low-cost units arranged periodically[5]; its main advantage is its flexible and powerful EM-wave management ability. RIS can be programmed using appropriate software to achieve real-time control of the EM environment, thus providing high capacity, coverage, and energy efficiency in future wireless networks. Given that RIS is inexpensive, easy to fabricate, and can be conveniently integrated and deployed in wireless communication systems, it is considered a promising technology that enhances the performance of mmWave 6G communication systems.

Extensive research on the performance of RIS-assisted mmWave wireless communication networks in various scenarios has been conducted. In Refs. [6-7], where RIS was used for beamforming and broadcasting, large-scale fading models were constructed, and measurement validation was conducted. To improve the spatial reuse of line-of-sight (LoS) mmWave systems, multiple RISs were introduced in Ref. [8] to customize the rank and truncated condition numbers of wireless channels. In Ref. [9], the coverage performance of mmWave systems was analyzed using the Saleh-Valenzuela model. In Ref. [10], RIS elements were activated during a pilot training

**Received** 2024-05-05, **Revised** 2024-09-09.

**Biographies**: Ai Junjie (2001—), male, Ph. D. candidate; Jin Shi (corresponding author), male, doctor, professor, jinshi@seu. edu. cn.

**Foundation items**: The National Natural Science Foundation of China (No. 62261160576, 62401137), the China Postdoctoral Science Foundation (No. BX20230065, 2024M750421), the Natural Science Foundation of Jiangsu Province (No. BK20241281), the Jiangsu Excellent Postdoctoral Program (No. 2023ZB476), the Fundamental Research Funds for the Central Universities (No. 2242023K5003), the Youth Science & Technology Talents Lifting Project by JSAST (No. TJ-2022-083).

**Citation**: AI Junjie, CHEN Weicong, LIU Jia, et al. Multiuser transmission scheme in millimeter-wave systems assisted by an RIS subarray[J]. Journal of Southeast University (English Edition), 2025, 41 (2): 140-146. DOI: 10. 3969/j. issn. 1003-7985. 2025. 02. 002.

process, and high-accuracy channel estimation was achieved using deep-learning methods. A widely spaced multisubarray deployment scheme for single-user equipment (UE) was proposed in Ref. [11] to enhance the spatial multiplexing gain of RIS-assisted multiple-input multiple-output (MIMO) systems. Regarding distributed MIMO wireless communication channels, an optimal frequency guide format that satisfies time-frequency separability and optimizes the peak-to-average power of the transmitted signal was proposed in Ref. [12].

In this work, we consider multiuser scenarios using the RIS subarray architecture and study the performance of subarray deployment strategies. Initially, we introduce a multiuser channel model in RIS-assisted mmWave MIMO systems. Based on this model, limited channel rank is achieved using a compact RIS architecture. To improve spatial multiplexing, we divide a compact RIS array into multiple widely spaced RIS subarrays. This design converts the far-field channel between a base station (BS) and RIS into a near-field channel. To minimize interuser interference, we deploy RIS subarrays in the discrete Fourier transform (DFT) direction of the BS antenna array. Using the proposed RIS subarray deployment strategies, the BS precoding, RIS reflection coefficient matrices, and the UE analog combiner are jointly designed to improve spectral efficiency (SE). Numerical simulation results demonstrate that in the four-user case, compared with the traditional compact RIS array, the proposed RIS subarray architecture and deployment strategy increase SEs of each UE and the total system by at least 3 and 20 bit/(s·Hz), respectively.

## 1 System Model

In this paper, we consider an RIS-assisted multiuser massive MIMO wireless communication system operating in the mmWave band. As shown in Fig. 1, the direct link between BS and $K_u$ UEs is blocked by obstacles; an RIS is deployed to create a virtual cascaded LoS link for wireless transmission. BS is a hybrid precoding system with a partially connected architecture; it consists of $K_b$ RF chains, each connected to $N_{ab}$ antennas. The vertical and horizontal spacings of the $N_b = K_b N_{ab}$ BS antennas are assumed to be $d = \lambda/2$, where $\lambda$ is the operating wavelength. RIS consists of $N_r$ elements, which are divided into $K_r$ subarrays, each containing $N_{ar}$ elements. The spacing between the antennas within each subarray is $d$, and the distance between subarrays is adjustable. UEs receive signals using an analog array consisting of $N_{au}$ antennas, where the antenna spacings are $d$. Considering that each UE can only receive one data stream, in this paper, we assume $K_b = K_r = K_u$.

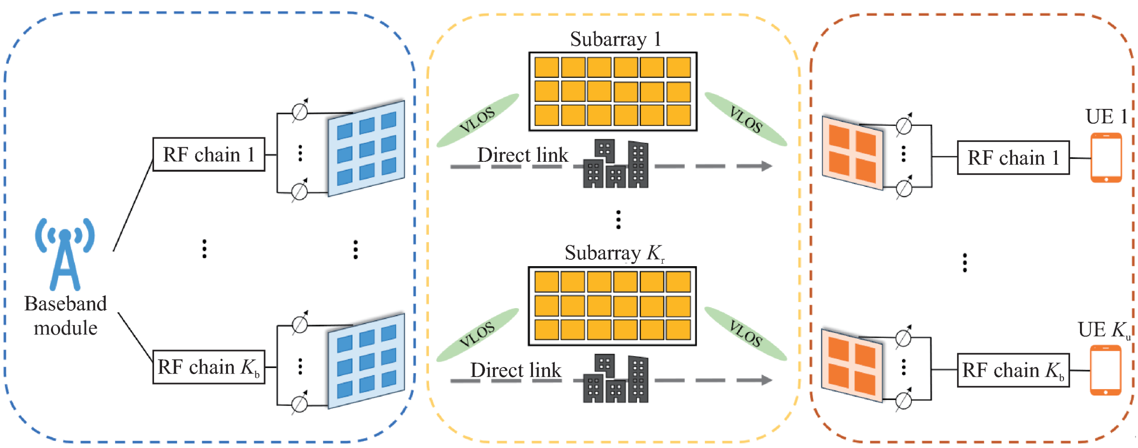


**Fig. 1** RIS-assisted massive MIMO wireless communication system

The signal received by the $k$-th UE can be expressed as

$$y_k = \boldsymbol{w}_{\mathrm{RF},k}^{\mathrm{H}} \boldsymbol{H}_k \boldsymbol{F}_{\mathrm{RF}} \boldsymbol{f}_{\mathrm{BB},k} s_k + \boldsymbol{w}_{\mathrm{RF},k}^{\mathrm{H}} \boldsymbol{H}_k \sum_{i \neq k} \boldsymbol{F}_{\mathrm{RF}} \boldsymbol{f}_{\mathrm{BB},i} s_i + \boldsymbol{w}_{\mathrm{RF},k}^{\mathrm{H}} \boldsymbol{n}_k \tag{1}$$

where $\boldsymbol{w}_{\mathrm{RF},k} \in \mathbf{C}^{N_{au} \times 1}$ denotes the analog combiner at the $k$-th UE; $\boldsymbol{H}_k \in \mathbf{C}^{N_{au} \times N_b}$ is the cascade channel between BS and the $k$-th UE; $\boldsymbol{F}_{\mathrm{RF}} = \mathrm{diag}\{\boldsymbol{f}_{\mathrm{RF},1}, \boldsymbol{f}_{\mathrm{RF},2}, \cdots, \boldsymbol{f}_{\mathrm{RF},K_b}\} \in \mathbf{C}^{N_b \times K_b}$ and $\boldsymbol{f}_{\mathrm{BB},k} \in \mathbf{C}^{K_b \times 1}$ denote the BS analog and digital precoders, respectively; $s_k$ is the signal transmitted to the $k$-th UE; $\boldsymbol{n}_k \in \mathbf{C}^{N_{au} \times 1}$ denotes the additive Gaussian white noise.

Superimposing the signals received by all UEs, we obtain

$$\boldsymbol{y} = [y_1, y_2, \cdots, y_{K_u}]^{\mathrm{T}} = \boldsymbol{W}_{\mathrm{RF}}^{\mathrm{H}} \boldsymbol{H} \boldsymbol{F}_{\mathrm{RF}} \boldsymbol{F}_{\mathrm{BB}} \boldsymbol{s} + \boldsymbol{W}_{\mathrm{RF}}^{\mathrm{H}} \boldsymbol{n} \tag{2}$$

where $\boldsymbol{W}_{\mathrm{RF}} = \mathrm{diag}\{\boldsymbol{w}_{\mathrm{RF},1}, \boldsymbol{w}_{\mathrm{RF},2}, \cdots, \boldsymbol{w}_{\mathrm{RF},K_u}\} \in \mathbf{C}^{N_u \times K_u}$ and $\boldsymbol{H} = [\boldsymbol{H}_1, \boldsymbol{H}_2, \cdots, \boldsymbol{H}_{K_u}]^{\mathrm{T}} \in \mathbf{C}^{N_u \times N_b}$; $\boldsymbol{F}_{\mathrm{BB}} = [\boldsymbol{f}_{\mathrm{BB},1}, \boldsymbol{f}_{\mathrm{BB},2}, \cdots, \boldsymbol{f}_{\mathrm{BB},K_b}] \in \mathbf{C}^{K_b \times K_b}$ satisfies the power constraint $\|\boldsymbol{F}_{\mathrm{RF}} \boldsymbol{F}_{\mathrm{BB}}\|_{\mathrm{F}}^2 = K_b$; $\boldsymbol{s} = [s_1, s_2, \cdots, s_{K_b}]^{\mathrm{T}} \in \mathbf{C}^{K_b \times 1}$ satisfies $E[\boldsymbol{s}\boldsymbol{s}^{\mathrm{H}}] = P_t \boldsymbol{I}_{K_b}/K_b$, where $P_t$ is the power transmitted by BS; $\boldsymbol{n} = [\boldsymbol{n}_1^{\mathrm{T}}, \boldsymbol{n}_2^{\mathrm{T}}, \cdots, \boldsymbol{n}_{K_u}^{\mathrm{T}}]^{\mathrm{T}} \in \mathbf{C}^{N_u \times 1}$.

Considering that the direct channel is severely blocked, the cascaded channel $\boldsymbol{H}_k$ between BS and the

$k$-th UE can be expressed as

$$\boldsymbol{H}_k = \boldsymbol{Q}_k \boldsymbol{\Phi} \boldsymbol{G} \tag{3}$$

where $\boldsymbol{Q}_k \in \mathbf{C}^{N_{\mathrm{au}} \times N_{\mathrm{r}}}$ and $\boldsymbol{G} \in \mathbf{C}^{N_{\mathrm{r}} \times N_{\mathrm{b}}}$ represent the segmented channels from RIS to the $k$-th UE and to BS, respectively; $\boldsymbol{\Phi} = \mathrm{diag}\{\boldsymbol{\Phi}_1, \boldsymbol{\Phi}_2, \cdots, \boldsymbol{\Phi}_{K_{\mathrm{r}}}\} \in \mathbf{C}^{N_{\mathrm{r}} \times N_{\mathrm{r}}}$ denotes the RIS reflection coefficient matrix, where $\boldsymbol{\Phi}_k = \mathrm{diag}\{\mathrm{e}^{\mathrm{j}\phi_{k,1}}, \mathrm{e}^{\mathrm{j}\phi_{k,2}}, \cdots, \mathrm{e}^{\mathrm{j}\phi_{k,N_{\mathrm{ar}}}}\} \in \mathbf{C}^{N_{\mathrm{ar}} \times N_{\mathrm{ar}}}$ is the reflection coefficient matrix of the $k$-th RIS subarray and $\phi_{k,i} \in [0, 2\pi)$ is the reflection phase of the $i$-th element in the $k$-th RIS subarray.

When RIS subarrays are compactly deployed, i. e., the spacing $d$ between subarrays is small, the size of the entire RIS is relatively small and BS is located at the RIS far field. In mmWave systems where the LoS path dominates the channel, the BS-RIS channel can be modeled as

$$\boldsymbol{G} = \mathrm{e}^{-\mathrm{j}\frac{2\pi}{\lambda} D_0} \boldsymbol{a}_{\mathrm{r}} \boldsymbol{a}_{\mathrm{b}}^{\mathrm{H}} \tag{4}$$

where $D_0$ is the distance between the BS and RIS array centers; $\boldsymbol{a}_{\mathrm{r}} = \boldsymbol{a}_{N_{\mathrm{r}}}(\theta_{\mathrm{r}}, \varphi_{\mathrm{r}}) \in \mathbf{C}^{N_{\mathrm{r}}}$ and $\boldsymbol{a}_{\mathrm{b}} = \boldsymbol{a}_{N_{\mathrm{b}}}(\theta_{\mathrm{b}}, \varphi_{\mathrm{b}}) \in \mathbf{C}^{N_{\mathrm{b}}}$ represent the normalized array steering vectors of the BS and RIS array, respectively.

Without loss of generality, for an $N$-element planar array with azimuth and elevation angles $\theta$ and $\varphi$, respectively, the normalized array steering vector $\boldsymbol{a}_N(\theta, \varphi) \in \mathbf{C}^N$ can be expressed as

$$\boldsymbol{a}_N(\theta, \varphi) = \frac{1}{\sqrt{N}} [\mathrm{e}^{\mathrm{j}\frac{2\pi}{\lambda}\psi_1}, \cdots, \mathrm{e}^{\mathrm{j}\frac{2\pi}{\lambda}\psi_n}, \cdots, \mathrm{e}^{\mathrm{j}\frac{2\pi}{\lambda}\psi_N}]^{\mathrm{T}} \tag{5}$$

where $\psi_n = (n_x - 1) d \cos\varphi \sin\theta + (n_z - 1) d \cos\theta$ represents the wave length difference; $n_x$ and $n_z$ are the row and column indices, respectively, of the $n$-th antenna of a uniform planar array.

When the distance between RIS and UE is less than the Rayleigh distance ($2D^2/\lambda$), BS will be in the RIS near field; otherwise, it will be in the RIS far field; $D$ is the RIS maximum physical dimension. In scenarios where multiple UEs share the same BS-RIS channel, a compact RIS deployment may place BS in the far field, thus reducing the BS-RIS channel rank. This also reduces the overall cascaded channel rank, failing to meet the $r(\boldsymbol{H}) \geqslant K_{\mathrm{u}}$ condition in multistream transmission. Increasing the spacing between RIS subarrays, thus expanding the size of the entire RIS array, BS can be placed in the near field of the array, potentially increasing the BS-RIS channel rank.

To address the near- and far-field effects caused by the size of the RIS array, we employ the hybrid spherical- and planar-wave channel model proposed in Ref. [11]. This model consists of a planar-wave submodel within the subarray and a spherical-wave submodel among subarrays and is used for BS-RIS channel-$\boldsymbol{G}$ modeling

$$\boldsymbol{G}^{\mathrm{H}} = \left[ \frac{\lambda \mathrm{e}^{\mathrm{j}\frac{2\pi}{\lambda} D_{\mathrm{g},1}}}{4\pi D_{g,1}} \boldsymbol{a}_{\mathrm{b},1} \boldsymbol{a}_{\mathrm{r},1}^{\mathrm{H}}, \frac{\lambda \mathrm{e}^{\mathrm{j}\frac{2\pi}{\lambda} D_{\mathrm{g},2}}}{4\pi D_{g,2}} \boldsymbol{a}_{\mathrm{b},2} \boldsymbol{a}_{\mathrm{r},2}^{\mathrm{H}}, \cdots, \right.$$
$$\left. \frac{\lambda \mathrm{e}^{\mathrm{j}\frac{2\pi}{\lambda} D_{\mathrm{g},K_{\mathrm{r}}}}}{4\pi D_{g,K_{\mathrm{r}}}} \boldsymbol{a}_{\mathrm{b},K_{\mathrm{r}}} \boldsymbol{a}_{\mathrm{r},K_{\mathrm{r}}}^{\mathrm{H}} \right] \tag{6}$$

where $D_{\mathrm{g},k_{\mathrm{r}}}$ is the distance between BS and the $k_{\mathrm{r}}$-th RIS subarray in the LoS path, and subscript $g$ indicates that this distance is associated with channel $\boldsymbol{G}$; $\boldsymbol{a}_{\mathrm{r},k_{\mathrm{r}}} = \boldsymbol{a}_{N_{\mathrm{r}}}(\theta_{\mathrm{r},k_{\mathrm{r}}}, \varphi_{\mathrm{r},k_{\mathrm{r}}}) \in \mathbf{C}^{N_{\mathrm{ar}}}$ and $\boldsymbol{a}_{\mathrm{b},k_{\mathrm{r}}} = \boldsymbol{a}_{N_{\mathrm{b}}}(\theta_{\mathrm{b},k_{\mathrm{r}}}, \varphi_{\mathrm{b},k_{\mathrm{r}}}) \in \mathbf{C}^{N_{\mathrm{b}}}$ denote the normalized array steering vectors of the $k_{\mathrm{r}}$-th RIS subarray and BS, respectively.

When RIS subarrays are sparsely deployed, the channel between RIS and the $k$-th UE can be modeled as

$$\boldsymbol{Q}_k = \left[ \frac{\lambda \mathrm{e}^{-\mathrm{j}\frac{2\pi}{\lambda} D_{\mathrm{q},1,k}}}{4\pi D_{\mathrm{q},1,k}} \boldsymbol{a}_{\mathrm{u},k,1} \boldsymbol{a}_{\mathrm{r},k,1}^{\mathrm{H}}, \frac{\lambda \mathrm{e}^{-\mathrm{j}\frac{2\pi}{\lambda} D_{\mathrm{q},2,k}}}{4\pi D_{\mathrm{q},2,k}} \boldsymbol{a}_{\mathrm{u},k,2} \boldsymbol{a}_{\mathrm{r},k,2}^{\mathrm{H}}, \cdots, \right.$$
$$\left. \frac{\lambda \mathrm{e}^{-\mathrm{j}\frac{2\pi}{\lambda} D_{\mathrm{q},K_{\mathrm{r}},k}}}{4\pi D_{\mathrm{q},K_{\mathrm{r}},k}} \boldsymbol{a}_{\mathrm{u},k,K_{\mathrm{r}}} \boldsymbol{a}_{\mathrm{r},k,K_{\mathrm{r}}}^{\mathrm{H}} \right] \tag{7}$$

where $D_{\mathrm{q},k_{\mathrm{r}},k}$ is the distance between the $k_{\mathrm{r}}$-th RIS subarray and the $k$-th UE in the LoS path, and subscript $q$ indicates that this distance is associated with channel $\boldsymbol{Q}$; $\boldsymbol{a}_{\mathrm{u},k,k_{\mathrm{r}}} = \boldsymbol{a}_{N_{\mathrm{au}}}(\theta_{\mathrm{u},k,k_{\mathrm{r}}}, \varphi_{\mathrm{u},k,k_{\mathrm{r}}}) \in \mathbf{C}^{N_{\mathrm{au}}}$ and $\boldsymbol{a}_{\mathrm{r},k,k_{\mathrm{r}}} = \boldsymbol{a}_{N_{\mathrm{ar}}}(\theta_{\mathrm{r},k,k_{\mathrm{r}}}, \varphi_{\mathrm{r},k,k_{\mathrm{r}}}) \in \mathbf{C}^{N_{\mathrm{ar}}}$ denote the normalized array steering vectors at $k$-th UE and $k_{\mathrm{r}}$-th RIS subarray, respectively. Substituting Eqs. (6) and (7) into Eq. (3), we obtain

$$\boldsymbol{H}_k = \sum_{i=1}^{K_{\mathrm{r}}} V_{i,k} \boldsymbol{a}_{\mathrm{u},k,i} \boldsymbol{a}_{\mathrm{r},k,i}^{\mathrm{H}} \boldsymbol{\Phi}_i \boldsymbol{a}_{\mathrm{r},i} \boldsymbol{a}_{\mathrm{b},i}^{\mathrm{H}} \tag{8}$$

where $V_{i,k} = \lambda^2 \mathrm{e}^{-\mathrm{j}\frac{2\pi}{\lambda}(D_{\mathrm{g},i} + D_{\mathrm{q},i,k})} / (16\pi^2 D_{\mathrm{g},i} D_{\mathrm{q},i,k})$ denotes the large-scale fading factor of the channel between BS and the $k$-th UE via the $i$-th RIS subarray.

Eq. (8) shows that the channel rank upper limit of the cascaded channel between BS and the $k$-th UE increases from 1 to $K_{\mathrm{r}}$. To support multistream transmission with reduced inter-UE interference, we investigate the deployment strategy of RIS subarrays in the next section.

## 2 Multistream Transmission Scheme

In this section, we investigate a multistream transmission scheme to improve the average system SE. When the noise energy is sufficiently small compared with the signal and interference energy, the average system SE $C$ can be defined as

$$E[C] = E\left[\sum_{k=1}^{K_{\mathrm{u}}} C_k\right] = E\left[\sum_{k=1}^{K_{\mathrm{u}}} \log_2(1 + S_k)\right] \tag{9}$$

where $C_k$ is the SE of the $k$-th UE; $S_k$ is the signal-to-interference ratio (SIR) of the $k$-th UE and can be expressed as

$$S_k = \frac{\| \boldsymbol{w}_{\mathrm{RF},k}^{\mathrm{H}} \boldsymbol{H}_k \boldsymbol{f}_{\mathrm{BF},k} \|^2}{\sum_{i \neq k} \| \boldsymbol{w}_{\mathrm{RF},k}^{\mathrm{H}} \boldsymbol{H}_k \boldsymbol{f}_{\mathrm{BF},i} \|^2} =$$

$$\frac{\left\| \sum_{j=1}^{K_r} V_{j,k} (\boldsymbol{w}_{\mathrm{RF},k}^{\mathrm{H}} \boldsymbol{a}_{\mathrm{u},k,j})(\boldsymbol{a}_{\mathrm{r},k,j}^{\mathrm{H}} \boldsymbol{\Phi}_j \boldsymbol{a}_{\mathrm{r},j})(\boldsymbol{a}_{\mathrm{b},j}^{\mathrm{H}} \boldsymbol{f}_{\mathrm{BF},k}) \right\|^2}{\sum_{i \neq k} \left\| \sum_{j=1}^{K_r} V_{j,k} (\boldsymbol{w}_{\mathrm{RF},k}^{\mathrm{H}} \boldsymbol{a}_{\mathrm{u},k,j})(\boldsymbol{a}_{\mathrm{r},k,j}^{\mathrm{H}} \boldsymbol{\Phi}_j \boldsymbol{a}_{\mathrm{r},j})(\boldsymbol{a}_{\mathrm{b},j}^{\mathrm{H}} \boldsymbol{f}_{\mathrm{BF},i}) \right\|^2} \tag{10}$$

where $\boldsymbol{f}_{\mathrm{BF},k} = \boldsymbol{F}_{\mathrm{RF}} \boldsymbol{f}_{\mathrm{BB},k}$. Note that by increasing the quality of the desired signal at a UE or suppressing the interference signal received from other UEs, SIR can be enhanced, thus improving SE. However, SIRs of different UEs are coupled via the analog combining matrix $\boldsymbol{W}_{\mathrm{RF}}$, the reflection coefficient matrix $\boldsymbol{\Phi}$, and the precoder matrix $\boldsymbol{F}_{\mathrm{RF}} \boldsymbol{F}_{\mathrm{BB}}$.

In the following, to maximize Eq. (10), $\boldsymbol{W}_{\mathrm{RF}}$, $\boldsymbol{F}_{\mathrm{RF}} \boldsymbol{F}_{\mathrm{BB}}$, and $\boldsymbol{\Phi}$ are jointly designed to maximize the numerator term, i. e., the desired signal power received by each UE. The RIS subarray is deployed in the DFT location to improve the orthogonality of the channel while minimizing the denominator term, i. e., the multiuser interference.

### 2.1 Beamforming and RIS reflection coefficient matrix design

To align the beam emitted from the subarray via the LoS path with the $k$-th UE, it is necessary to design the RIS reflection coefficient matrix, the UE analog combiner, and the BS precoder. This design ensures that the beam energy at the UE location is maximized, as indicated in Eq. (10). Thus, the analog combining vector $\boldsymbol{w}_{\mathrm{RF},k}$ for the $k$-th UE and the phase matrix $\boldsymbol{\Phi}_k$ for the $k$-th subarray of the RIS can be designed as

$$\boldsymbol{w}_{\mathrm{RF},k} = \boldsymbol{a}_{\mathrm{u},k,k} \tag{11}$$

$$\boldsymbol{a}_{\mathrm{r},k,k}^{\mathrm{H}} \boldsymbol{\Phi}_k \boldsymbol{a}_{\mathrm{r},k} = 1 \tag{12}$$

Substituting the expressions for the array steering vectors into Eq. (12), we obtain

$$\phi_{k,i} = \frac{2\pi}{\lambda} (\psi_{\mathrm{r},k,i,\mathrm{AOD}} - \psi_{\mathrm{r},k,i,\mathrm{AOA}}) \tag{13}$$

Considering that the BS precoder matrix must satisfy

$$\max\{\boldsymbol{a}_{\mathrm{b},j}^{\mathrm{H}} \boldsymbol{f}_{\mathrm{BF},i}, i = j\} \tag{14}$$

Hence, when $\boldsymbol{F}_{\mathrm{BB}} = \boldsymbol{I}_{K_b}$, the expression for the one-column vector $\boldsymbol{f}_{\mathrm{RF},i}$ in $\boldsymbol{F}_{\mathrm{BF}}$ can be obtained as

$$\boldsymbol{f}_{\mathrm{RF},i} = [\boldsymbol{a}_{\mathrm{b},i,x}] \otimes [\boldsymbol{a}_{\mathrm{b},i,z}] \tag{15}$$

where $\otimes$ represents the Kronecker product operation; $\boldsymbol{a}_{\mathrm{b},i,x} = \boldsymbol{a}_{N_{\mathrm{ab}x}}(\theta_{\mathrm{b},i}, \varphi_{\mathrm{b},i}) \in \mathbf{C}^{N_{\mathrm{ab}x}}$ and $\boldsymbol{a}_{\mathrm{b},i,z} = \boldsymbol{a}_{N_{\mathrm{ab}z}}(\theta_{\mathrm{b},i}, \varphi_{\mathrm{b},i}) \in \mathbf{C}^{N_{\mathrm{ab}z}}$ denote the array steering vectors in the $x$- and $z$-axis, respectively, formed by BS in the $i$-th RIS subarray; $N_{\mathrm{ab}x}$ and $N_{\mathrm{ab}z}$ denote the number of antennas in the $x$- and $z$-axis, respectively, within BS, satisfying $N_{\mathrm{ab}} = N_{\mathrm{ab}x} N_{\mathrm{ab}z}$.

Furthermore, it can be derived that

$$\boldsymbol{a}_{\mathrm{b},i}^{\mathrm{H}} \boldsymbol{f}_{\mathrm{BF},i} = \frac{1}{\sqrt{N_{\mathrm{b}} N_{\mathrm{ab}}}} \sum_{n_x=1}^{N_{\mathrm{ab}x}} \sum_{n_z=1}^{N_{\mathrm{ab}z}} \mathrm{e}^{-\mathrm{j}\left[(n_x-1)\frac{2\pi}{\lambda} d(\cos\varphi_{\mathrm{b},i}\sin\theta_{\mathrm{b},i} - \cos\varphi_{\mathrm{b},i}\sin\theta_{\mathrm{b},i}) + (n_z-1)\frac{2\pi}{\lambda} d(\cos\theta_{\mathrm{b},i} - \cos\theta_{\mathrm{b},i})\right]} = \frac{N_{\mathrm{ab}}}{\sqrt{N_{\mathrm{b}} N_{\mathrm{ab}}}} = \sqrt{\frac{1}{K_{\mathrm{b}}}} \tag{16}$$

### 2.2 RIS subarray position deployment scheme

To minimize interference, it is necessary to design the deployment locations of the BS arrays and RIS subarrays in such a way that each subchannel is orthogonal to each other, i. e., the following must be satisfied:

$$\boldsymbol{a}_{\mathrm{b},j}^{\mathrm{H}} \boldsymbol{f}_{\mathrm{BF},i} = \frac{1}{\sqrt{N_{\mathrm{b}} N_{\mathrm{ab}}}} \sum_{n_x=1}^{N_{\mathrm{ab}x}} \mathrm{e}^{-\mathrm{j}(n_x-1)\frac{2\pi}{\lambda} d(\cos\varphi_{\mathrm{b},j}\sin\theta_{\mathrm{b},j} - \cos\varphi_{\mathrm{b},i}\sin\theta_{\mathrm{b},i})} \sum_{n_z=1}^{N_{\mathrm{ab}z}} \mathrm{e}^{-\mathrm{j}(n_z-1)\frac{2\pi}{\lambda} d(\cos\theta_{\mathrm{b},j} - \cos\theta_{\mathrm{b},i})} = 0 \tag{17}$$

Using $\sum_{n=1}^{N} \mathrm{e}^{\mathrm{j}(n-1)\alpha} = \mathrm{e}^{\mathrm{j}\alpha(N-1)/2} \sin(N\alpha/2)/\sin(\alpha/2)$, Eq. (17) can be equivalently written as

$$\begin{cases} \dfrac{N_{\mathrm{ab}z}}{2} \dfrac{2\pi}{\lambda} d(\cos\theta_{\mathrm{b},j} - \cos\theta_{\mathrm{b},i}) = \pm k\pi & k \in \mathbf{N}^+ \\ \dfrac{N_{\mathrm{ab}x}}{2} \dfrac{2\pi}{\lambda} d(\cos\varphi_{\mathrm{b},j}\sin\theta_{\mathrm{b},j} - \cos\varphi_{\mathrm{b},i}\sin\theta_{\mathrm{b},i}) = \\ \pm k\pi & k \in \mathbf{N}^+ \end{cases} \tag{18}$$

Reorganizing the above equation and considering the case of $K_{\mathrm{u}} = 4$ as an example, which can be generalized in multiuser scenarios with any number of UEs, the angular parameters between BS and the RIS subarrays at this point satisfy

$$\begin{cases} \cos\theta_{\mathrm{b},1} - \cos\theta_{\mathrm{b},2} = \dfrac{\pm i_2 \lambda}{N_{\mathrm{ab}z} d} & i_2 = 1, 2, \cdots \\ \cos\theta_{\mathrm{b},1} - \cos\theta_{\mathrm{b},3} = \dfrac{\pm i_3 \lambda}{N_{\mathrm{ab}z} d} & i_3 = 1, 2, \cdots \\ \cos\theta_{\mathrm{b},1} - \cos\theta_{\mathrm{b},4} = \dfrac{\pm i_4 \lambda}{N_{\mathrm{ab}z} d} & i_4 = 1, 2, \cdots \end{cases} \tag{19}$$

$$\begin{cases} \cos\varphi_{\mathrm{b},2}\sin\theta_{\mathrm{b},2} - \cos\varphi_{\mathrm{b},1}\sin\theta_{\mathrm{b},1} = \dfrac{\pm i_2 \lambda}{N_{\mathrm{ab}x} d} \\ i_2 = 1, 2, \cdots \\ \cos\varphi_{\mathrm{b},3}\sin\theta_{\mathrm{b},3} - \cos\varphi_{\mathrm{b},1}\sin\theta_{\mathrm{b},1} = \dfrac{\pm i_3 \lambda}{N_{\mathrm{ab}x} d} \\ i_3 = 1, 2, \cdots \\ \cos\varphi_{\mathrm{b},4}\sin\theta_{\mathrm{b},4} - \cos\varphi_{\mathrm{b},1}\sin\theta_{\mathrm{b},1} = \dfrac{\pm i_4 \lambda}{N_{\mathrm{ab}x} d} \\ i_4 = 1, 2, \cdots \end{cases} \tag{20}$$

It can be further deduced that the channels between BS and the RIS subarrays are orthogonal to each other when the deployment position of an RIS subarray satisfies

$$\begin{cases} x_{\mathrm{r},j} = \cot\varphi_{\mathrm{b},j}(y_{\mathrm{r},j} - y_{\mathrm{b}}) + x_{\mathrm{b}} \\ y_{\mathrm{r},j} = D_{\text{BS-RIS}} \\ z_{\mathrm{r},j} = z_{\mathrm{b}} + \sqrt{(x_{\mathrm{r},j} - x_{\mathrm{b}})^2 + (y_{\mathrm{r},j} - y_{\mathrm{b}})^2} \cot\theta_{\mathrm{b},j} \end{cases} \tag{21}$$

The process of obtaining the deployment coordinates of the RIS subarray is summarized as follows. Using the

BS position and its communication distance to the RIS array, the elevation and azimuth angles of the RIS subarray relative to BS can be calculated using Eqs. (19) and (20). Subsequently, this angular information is substituted into Eq. (21) to derive the final coordinates.

## 3 Numerical Simulation

In this section, we evaluate the SE and effective rank of the system based on the above RIS subarray deployment scheme. Additionally, we compare the advantages of the proposed scheme over the traditional RIS subarray compact deployment scheme.

In the simulation setup, we consider the case $K_{\mathrm{b}} = K_{\mathrm{r}} = K_{\mathrm{u}} = 4$, and the antenna spacing within each subarray is $\lambda/2$. BS has $N_{\mathrm{b}} = 100$ antennas, and each RF chain controls a $5 \times 5$ antenna array. RIS consists of $N_{\mathrm{r}} = 256$ elements, where the subarray size is $8 \times 8$ and the subarray Rayleigh distance is 0.69 m. Each UE receives signals via a $2 \times 2$ antenna array. There are $L_{\mathrm{u}} = 2$ randomly distributed scattering elements between RIS and UEs. The system operates at a frequency $f = 28$ GHz with a bandwidth $W = 10$ GHz. The total transmitted power is $P_{\mathrm{t}} = 1$ dBW, and the noise at each UE is thermal noise with a variance $\sigma_{\mathrm{N}}^2 = 4 \times 10^{-11}$.

The effective rank of the BS-RIS channel matrix $\boldsymbol{G}$ and the SE are analyzed when the RIS subarrays are deployed in a colinear and a coplanar configuration, respectively. In the colinear case, for simplicity, we set $\cos\varphi_{\mathrm{b}} = 0$ and $\cos\theta_{\mathrm{b},2} = 0$; in the coplanar case, we set $\cos\theta_{\mathrm{b},2} = \cos\varphi_{\mathrm{b},2} = 0$. Based on Eqs. (19) and (20), the elevation and azimuth angles can be obtained to satisfy Eqs. (22) and (23) for these two cases, respectively. Furthermore, the central position of the RIS subarrays can be calculated using Eq. (21).

$$\begin{cases} \cos\theta_{\mathrm{b},2} - \cos\theta_{\mathrm{b},1} = \dfrac{\lambda}{N_{\mathrm{ab}x} d} \\ \cos\theta_{\mathrm{b},3} - \cos\theta_{\mathrm{b},2} = \dfrac{\lambda}{N_{\mathrm{ab}x} d} \\ \cos\theta_{\mathrm{b},4} - \cos\theta_{\mathrm{b},3} = \dfrac{\lambda}{N_{\mathrm{ab}x} d} \end{cases} \tag{22}$$

$$\begin{cases} \cos\theta_{\mathrm{b},1} = \dfrac{-\lambda}{N_{\mathrm{ab}z} d}, \quad \cos\varphi_{\mathrm{b},1} = \dfrac{\lambda}{N_{\mathrm{ab}x} d \sin\theta_{\mathrm{b},1}} \\ \cos\theta_{\mathrm{b},3} = \dfrac{\lambda}{N_{\mathrm{ab}z} d}, \quad \cos\varphi_{\mathrm{b},3} = \dfrac{\lambda}{N_{\mathrm{ab}x} d \sin\theta_{\mathrm{b},3}} \\ \cos\theta_{\mathrm{b},4} = \dfrac{2\lambda}{N_{\mathrm{ab}z} d}, \quad \cos\varphi_{\mathrm{b},4} = \dfrac{-\lambda}{N_{\mathrm{ab}x} d \sin\theta_{\mathrm{b},4}} \end{cases} \tag{23}$$

The deployment of the BS and RIS subarrays is shown in Fig. 2; the red circles, green asterisks, and blue cycles represent the BS antenna positions, the BS antenna array central positions, and the RIS subarray central positions, respectively. The Rayleigh distances between BS and the two RIS array deployment schemes are 15.1 and 31.8 km, respectively. The distance between the BS and RIS array is set to $D_{\text{BS-RIS}} = 5$ m, and the distance between RIS and UE follows a uniform distribution $D_{\text{RIS-UE}} \sim U(5, 100)$. The $x$ and $z$ coordinates of each UE satisfy $|x|, |z| \sim U(0, 10)$, i. e., UEs and BS are located in the near field of the RIS array and the far field of the RIS subarray.

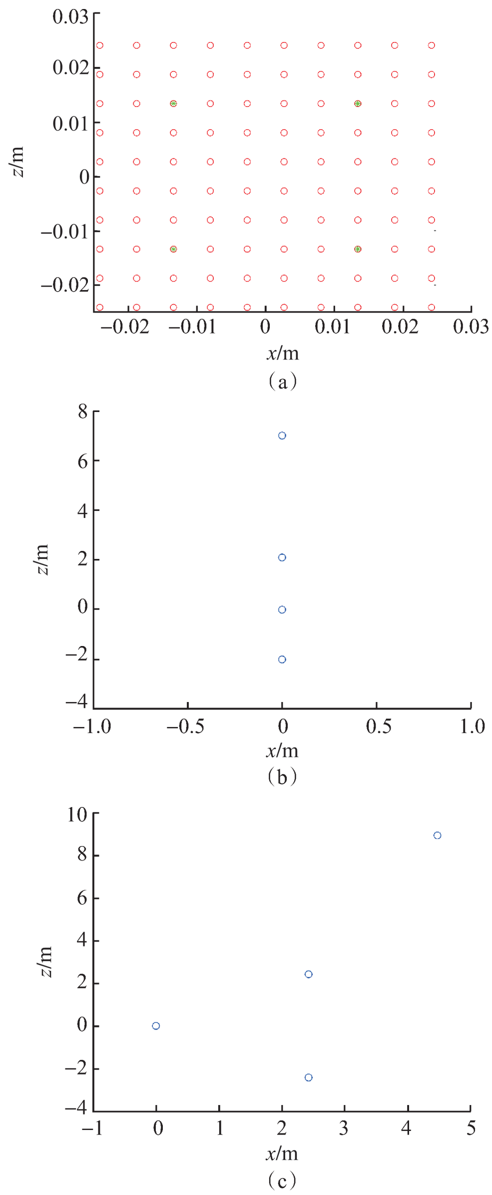


**Fig. 2** Deployment cases of the BS and RIS subarrays. (a) BS; (b) Colinear; (c) Coplanar

The values of $|\boldsymbol{a}_{\mathrm{b},j}^{\mathrm{H}} \boldsymbol{f}_{\mathrm{BF},i}|$ $(i, j = 1, 2, 3, 4)$ considering colinear and coplanar deployment were obtained using simulation and recorded in Table 1 and Table 2, respectively. We observe that when $i = j$, $|\boldsymbol{a}_{\mathrm{b},j}^{\mathrm{H}} \boldsymbol{f}_{\mathrm{BF},i}| = \sqrt{1/K_{\mathrm{b}}} = 0.5$. When $i \neq j$, $|\boldsymbol{a}_{\mathrm{b},j}^{\mathrm{H}} \boldsymbol{f}_{\mathrm{BF},i}|$ is significantly smaller than

0.5 approaching 0. Furthermore, the effective rank[13] of the BS-RIS channel in the colinear and coplanar deployment can be obtained as rank($\boldsymbol{G}$) ≈ 3.93 and rank($\boldsymbol{G}$) ≈ 3.85, respectively. These results confirm that the proposed system configuration and RIS subarray deployment scheme increase channel rank to support multistream transmission.

**Table 1** Simulated values of $|\boldsymbol{a}_{\mathrm{b},j}^{\mathrm{H}}\boldsymbol{f}_{\mathrm{BF},i}|$ in the RIS subarray colinear deployment

| j | i = 1 | i = 2 | i = 3 | i = 4 |
|---|---|---|---|---|
| 1 | 0.5 | $1.3\times10^{-16}$ | $8.3\times10^{-17}$ | $7.8\times10^{-17}$ |
| 2 | $1.6\times10^{-16}$ | 0.5 | $1.6\times10^{-16}$ | $4.2\times10^{-17}$ |
| 3 | $8.3\times10^{-17}$ | $1.3\times10^{-16}$ | 0.5 | $7.6\times10^{-17}$ |
| 4 | $1.1\times10^{-16}$ | $4.3\times10^{-17}$ | $7.7\times10^{-17}$ | 0.5 |

**Table 2** Simulated values of $|\boldsymbol{a}_{\mathrm{b},j}^{\mathrm{H}}\boldsymbol{f}_{\mathrm{BF},i}|$ in the RIS subarray coplanar deployment

| j | i = 1 | i = 2 | i = 3 | i = 4 |
|---|---|---|---|---|
| 1 | 0.5 | $1.4\times10^{-17}$ | $3.1\times10^{-17}$ | $1.1\times10^{-17}$ |
| 2 | $1.4\times10^{-17}$ | 0.5 | $7.8\times10^{-18}$ | $1.7\times10^{-18}$ |
| 3 | $2.4\times10^{-17}$ | $6.9\times10^{-18}$ | 0.5 | $6.7\times10^{-17}$ |
| 4 | $7.8\times10^{-17}$ | $5.5\times10^{-18}$ | $1.4\times10^{-17}$ | 0.5 |

Further, the SE of each UE and the system SE were calculated using Eq. (9). By performing a Monte Carlo simulation, we obtained the cumulative distribution function (CDF) of SE for each UE in different scenarios such as RIS subarray colinear deployment, RIS subarray coplanar deployment, and RIS compact deployment. The SE results for individual UEs and the overall system are shown in Figs. 3 and 4, respectively.

Figs. 3 and 4 show that, compared with the compact RIS, by deploying an RIS subarray architecture according to the DFT position scheme, the SE of a single UE and the entire system SE exceed 3 and 20 bit/(s·Hz), achieving a significant improvement in system performance.

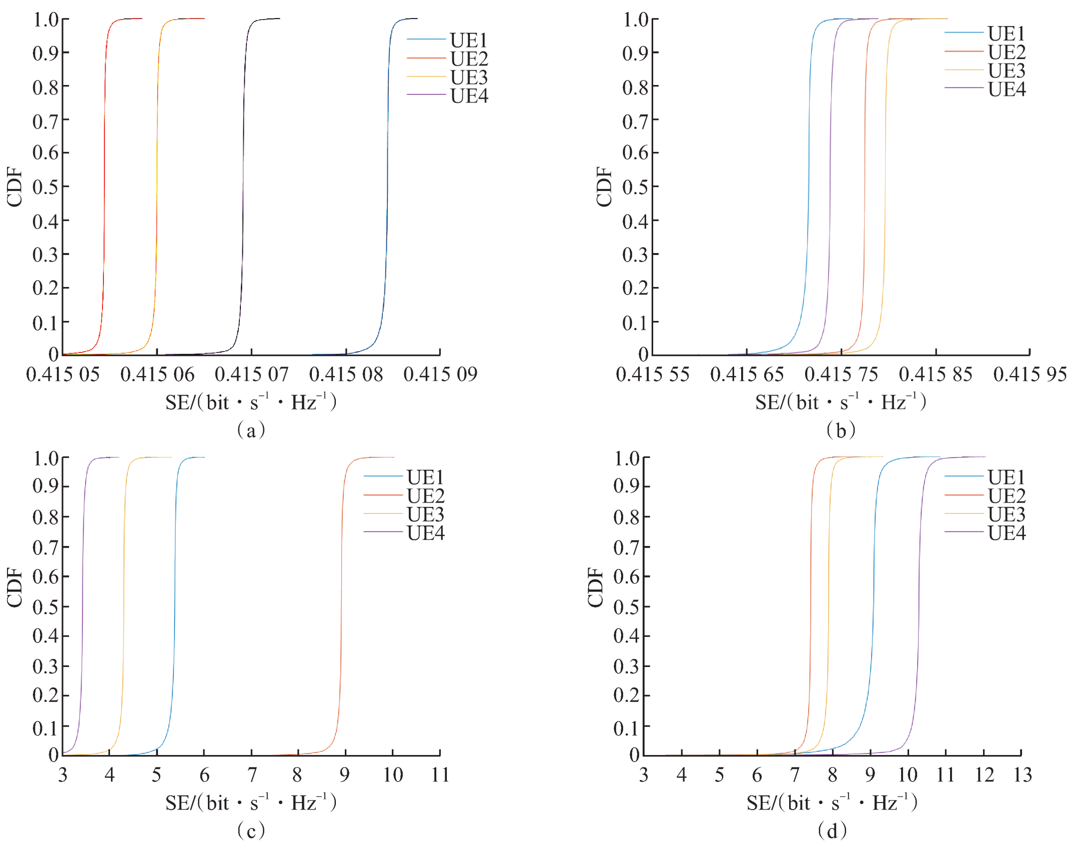


**Fig. 3** CDF of SE for each UE in the proposed RIS deployment. (a) Colinear and compact deployment; (b) Coplanar and compact deployment; (c) Colinear and subarray deployment; (d) Coplanar and subarray deployment

## 4 Conclusions

(1) By expanding a compact RIS array into a subarray structure and deploying it at DFT positions, UE interference can be minimized. Additionally, joint-beam alignment between BS, RIS, and UEs can maximize the signal energy received by each UE.

(2) The RIS subarray structure increases the effective rank of the cascaded channel, approaching full rank, thereby enhancing spatial multiplexing and multistream transmission.

(3) The proposed wireless transmission scheme with the RIS subarray structure increases the SE of a single UE by over 3 bit/(s·Hz), boosting the total SE by over 20 bit/(s·Hz).

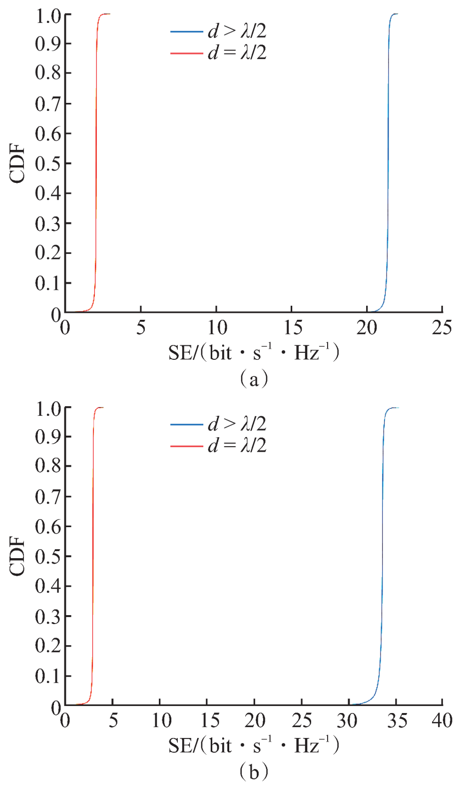


**Fig. 4** CDF of total SE of UEs in proposed RIS deployment. (a) Colinear deployment; (b) Coplanar deployment

## References


[1] ZHANG H, CHEN L Q, YANG B, et al. Secure lightweight data using scheme in 5G industrial Internet systems[J]. Journal of Southeast University (Natural Science Edition), 2024, 54(3): 772-780. (in Chinese)

[2] SAAD W, BENNIS M, CHEN M Z. A vision of 6G wireless systems: Applications, trends, technologies, and open research problems[J]. IEEE Network, 2020, 34(3): 134-142.

[3] RAPPAPORT T S, SUN S, MAYZUS R, et al. Millimeter wave mobile communications for 5G cellular: It will work![J]. IEEE Access, 2013, 1: 335-349.

[4] NIU Y, LI Y, JIN D P, et al. A survey of millimeter wave communications (mmWave) for 5G: Opportunities and challenges[J]. Wireless Networks, 2015, 21(8): 2657-2676.

[5] YANG L L, QIN T, TU Y, et al. Simulation study on retinal imaging display based on meta-surface micro-nano structures[J]. Journal of Southeast University (Natural Science Edition), 2024, 54(4): 990-996. (in Chinese)

[6] TANG W K, CHEN M Z, CHEN X Y, et al. Wireless communications with reconfigurable intelligent surface: Path loss modeling and experimental measurement[J]. IEEE Transactions on Wireless Communications, 2021, 20(1): 421-439.

[7] TANG W K, CHEN X Y, CHEN M Z, et al. Path loss modeling and measurements for reconfigurable intelligent surfaces in the millimeter-wave frequency band[J]. IEEE Transactions on Communications, 2022, 70 (9) : 6259-6276.

[8] CHEN W C, WEN C K, LI X, et al. Channel customization for joint Tx-RISs-Rx design in hybrid mmWave systems[J]. IEEE Transactions on Wireless Communications, 2023, 22(11): 8304-8319.

[9] LI R W, SUN S, CHEN Y H, et al. Ergodic achievable rate analysis and optimization of RIS-assisted millimeter-wave MIMO communication systems [J]. IEEE Transactions on Wireless Communications, 2023, 22(2): 972-985.

[10] LIU S C, GAO Z, ZHANG J, et al. Deep denoising neural network assisted compressive channel estimation for mmWave intelligent reflecting surfaces[J]. IEEE Transactions on Vehicular Technology, 2020, 69(8): 9223-9228.

[11] CHEN Y H, LI R W, HAN C, et al. Hybrid spherical- and planar-wave channel modeling and estimation for terahertz integrated UM-MIMO and IRS systems [J]. IEEE Transactions on Wireless Communications, 2023, 22(12): 9746-9761.

[12] WANG H M, ZHANG H, ZHANG N Z, et al. Optimal pilot design for distributed MIMO channel measurement systems[J]. Journal of Southeast University (Natural Science Edition), 2014, 44(1): 19-22. (in Chinese)

[13] ROY O, VETTERLI M. The effective rank: A measure of effective dimensionality[C]//2007 15th European Signal Processing Conference. Poznan, Poland, 2007: 606-610.


# 智能超表面子阵辅助的毫米波多用户传输方案


艾俊杰，陈伟聪，刘葭，蔡雪峰，唐万恺，金石

（东南大学移动通信全国重点实验室，南京 211189）



**摘要**：部署智能超表面可增强毫米波通信覆盖能力，但基站与超表面间典型的强视距远场传播将降低信道秩，影响多用户空间复用。针对以上挑战，提出了智能超表面子阵辅助的毫米波多用户传输方案。为了提高信道秩，将智能超表面被划分成多个具有可调间距的子阵，并且采用混合球面波和平面波模型进行信道建模。从最小化多用户间干扰的目标出发，将智能超表面子阵部署于基站的DFT方向上。基于最大化有效信号的准则，联合设计了基站的预编码、智能超表面的反射系数以及用户的合并矩阵。数值仿真验证了所提智能超表面子阵部署策略的有效性以及无线传输方案的性能。在毫米波频段四用户的通信场景下，基站与智能超表面间信道的有效秩在接近满秩的同时，各用户的频谱效率均获得至少3 bit/(s·Hz)的提升。



**关键词**：毫米波；智能超表面；DFT码本；无线通信

**中图分类号**：TN929.5